energies

MDPI

Article

Characteristics of Fracturing Fluid Invasion Layer and Its Influence on Gas Production of Shale Gas Reservoirs

Shijun Huang [1], Jiaojiao Zhang [1,*], Jin Shi [2], Fenglan Zhao [1] and Xianggang Duan [3]

[1] College of Petroleum Engineering, China University of Petroleum Beijing, Beijing 102249, China
[2] Shelfoil Petroleum Equipment and Services Co., Ltd., Dezhou 253034, China
[3] PetroChina Research Institute of Petroleum Exploration and Development, Beijing 100083, China
* Correspondence: zhangjiaojiao2198@163.com

Abstract: With the increase of shale gas resource exploitation in our country during recent decades, the situations of low gas production, fast production decline rate, and low flowback rate have been appearing in field production. It is an urgent problem to be solved in shale gas production and it is therefore necessary to study the interaction of the shale gas reservoir and the detained fracturing fluid. In this paper, the Longmaxi Formation shale samples of Sichuan Basin were selected for a water invasion experiment. The fracture propagation law, the water invasion front location, and the water invasion thickness of deep and shallow shale reservoirs after water invasion were compared and analyzed by CT scanning technology. Based on the analysis of the experimental mechanism, a numerical simulation model was established. The dimensionless permeability and thickness of the fracturing fluid invasion layer were introduced to analyze the positive and negative effects of fracturing fluid retention on the reservoir. The results show that during the hydraulic fracturing of shale gas wells, fracturing fluid can quickly enter the complex fracture network, and then slowly enter the shale matrix under various mechanisms to form the fracturing fluid invasion layer. Compared with shallow shale reservoirs, deep shale reservoirs have lower porosity and permeability, which propagates microfractures in the matrix induced by fracturing fluid retention, and results in a smaller fracturing fluid invasion layer thickness. Both the negative effect of fracturing fluid retention on shale damage and the positive effect of microfracture formation and propagation exist simultaneously. The higher the dimensionless fracturing fluid invasion layer permeability, the more complex the fracture network formed in the fractured reservoir will be, resulting in a longer stable production period and a better development effect. When the dimensionless fracturing fluid invasion layer permeability is greater than 1, that is, when the positive effect of fracturing fluid retention is greater, and the thicker the dimensionless fracturing fluid invasion layer is, the better the development effect will be. Combining reservoir characteristics and fracture development, the key to obtaining high productivity of a shale gas well is to optimize the soaking time and the speed of flowback in order to extend the stable production period. In this paper, the characteristics of the fracturing fluid invasion layer and the influence of fracturing fluid retention on gas well productivity are deeply studied, which provides a certain theoretical basis for the optimization of shale gas extraction technology and the improvement of the gas–water two-phase productivity prediction method for fractured horizontal wells.

Keywords: fracturing fluid retention; fracturing fluid invasion layer; CT scan; numerical simulation; shale gas reservoir

check for updates

Citation: Huang, S.; Zhang, J.; Shi, J.; Zhao, F.; Duan, X. Characteristics of Fracturing Fluid Invasion Layer and Its Influence on Gas Production of Shale Gas Reservoirs. *Energies* **2023**, *16*, 3924. https://doi.org/10.3390/en16093924

Academic Editor: Rouhi Farajzadeh

Received: 7 April 2023
Revised: 29 April 2023
Accepted: 3 May 2023
Published: 6 May 2023

Copyright: © 2023 by the authors. Licensee MDPI, Basel, Switzerland. This article is an open access article distributed under the terms and conditions of the Creative Commons Attribution (CC BY) license (https://creativecommons.org/licenses/by/4.0/).

1. Introduction

Marine shale gas resources are abundant in Sichuan Basin. After more than ten years of exploration and development, commercial development has been achieved in Fuling, Weiyuan-Changning, Zhaotong, and Jiaoshiba blocks [1,2]. The shale reservoir is tight with low porosity and permeability, so hydraulic fracturing technology is the necessary

means of industrial development. Tens of thousands of cubic meters of fracturing fluid are pumped into the shale reservoirs under high pressure during hydraulic fracturing [3,4], but field production data show that the flowback rate of fracturing fluid is generally lower than 30% [5,6]. A large amount of fracturing fluid remains in the reservoir and has physical and chemical interactions with the shale reservoir, which affects the matrix and fractures of the reservoir, and ultimately affects the gas permeability and productivity of the shale reservoir.

The retention of fracturing fluid in the shale reservoir is jointly controlled by various mechanisms [7–9], which can be mainly divided into two categories. One is that a complex fracture network is formed in the fractured reservoir after fracturing, and after fracturing fluid backflow, the pressure drops and the fracture is closed, resulting in a large amount of fracturing fluid remaining in the fracture network. Meanwhile, the surface of the fracture is rough and uneven, and capillary retention related to roughness will occur in the fracture. The other is that fracturing fluid enters the shale matrix through fractures under spontaneous imbibition. In addition, as fracturing fluid flows across the rock, it leaves behind a thin coating of water on the rock surface, causing fracturing fluid retention. Gravity also affects fracturing fluid retention. Moreover, fracturing fluid is a polymer solution with a crosslinked network structure that is prone to retention when flowing through porous media at low speeds [10]. Song [11] found that the retained fracturing fluid in the reservoir was distributed in artificial fractures, in open natural fractures or induced microfractures, and in the matrix around the fracture. Mcclure [12] studied hydraulic fractures and natural fractures by means of numerical simulation, and found that hydraulic fractures extend and connect with natural fractures during fracturing, and the stress field changes at the intersection, leading to the closure of fractures and the retention of fracturing fluid. Agrawal and Aharma [13] used a numerical simulation to study the influence of gravity on fracturing fluid flowback, and found that the flowback rate at the top of the fracture is higher than that at the bottom of the fracture in horizontal wells. Parmar et al. [14] found that gravity has a great influence on fracturing fluid retention, and surfactants can alter rock wettability and affect the flowback rate of a shale reservoir. Liu [15] found that matrix imbibition caused by capillary force would become more obvious when the effect of gravity was weakened. Paramar et al. [16] believed that capillary force and gravity would affect fluid flow in fractures, and well shut-in and reopening would lead to proppant crushing, thereby increasing the capillary force of the matrix and affecting the flowback of the remaining fracturing fluid in propped fractures. Fracturing fluid flowback in fractures below horizontal wells is opposite to the direction of gravity, resulting in a large amount of fracturing fluid detained at the bottom of the fracture. Cheng [17] found that with the increase of capillary force, the amount of imbibition in the matrix increased, the width of natural fractures increased, and the water retention increased. Penny et al. [18] believed that the conductivity of artificial fractures was very high and the capillary force could be ignored during hydraulic fracturing, but the capillary force in natural fractures and the matrix was very large, which could cause water to enter and be retained. King [19] found that fracture complexity was the main reason for the low flowback rate of fracturing fluid. Warpinski et al. [20] and Mark McClure and Horne [21] found that low fracture conductivity was not conducive to fracturing fluid flowback, and the higher the fracturing fluid flowback rate, the more complex the fracture network formed after hydraulic fracturing would be. Modeland et al. [22] found that proppant crushing reduced the conductivity of fractures, resulting in a lower flowback rate during production of a shale reservoir.

At present, the research on the impact of fracturing fluid on shale reservoirs is mainly focused on the study of microscopic pore structure change and the fracture propagation rule by means of scanning electron microscopes; nuclear magnetic resonance and CT scanning; the test of macroscopic parameters such as porosity, permeability, and mechanical properties before and after imbibition of fracturing fluid; and the influence of fracturing fluid retention on oil and gas migration and ultimate recovery [23–27]. Domestic and foreign scholars have not reached a consensus on the impact of retained fracturing fluid on the reservoir. Most scholars believe that fracturing fluid intrusion will damage shale reservoirs and

reduce gas production, which is mainly shown in the following features [28,29]. The permeability and porosity of shale reservoirs are low, so they are prone to water block damage [30]. The hydration and swelling of clay minerals easily occur in shale reservoirs with high clay content [31,32]. The mechanical properties of shale reservoirs change obviously after hydration, and the brittleness and strength of shale reservoirs decrease after water invasion [33]. The solid residue of fracturing fluid and the precipitates formed by shale–liquid interaction gather in the fracture, resulting in the decrease of fracture conductivity [34]. However, some scholars believe that the imbibition of fracturing fluid into the shale reservoir will improve the pore structure, expand and connect microfractures, increase the permeability and porosity around fractures, and thus improve the productivity of shale gas wells [35–37]. Field production shows that the flowback rate of fracturing fluid is closely related to the production of a gas well, and the result of the interaction between shale and the retained fracturing fluid in different blocks is also different. Therefore, it is necessary to further study the effects of retained fracturing fluid on a reservoir based on the geological conditions and fluid physical parameters of the specific reservoir.

This study examined the shale gas reservoir of the Longmaxi Formation in the Sichuan Basin. By using CT scanning technology, the law of fracture propagation, the location of the water invasion front, and the thickness of the water invasion layer in deep and shallow shale reservoirs were compared and analyzed. Based on the experiments, the dimensionless permeability and thickness of the fracturing fluid invasion layer were introduced to study the influence of the fracturing fluid invasion layer characteristics on pressure and production by numerical simulation combined with specific block characteristics, and the favorable and unfavorable effects of fracturing fluid retention on the reservoir were defined.

2. Experimental Study

Core samples from different blocks were used for the water invasion simulation experiment, and core samples at various times were selected for CT scanning test during the experiment to observe the fracture propagation rule and to locate the water invasion frontier in the matrix, and to determine the characteristics of the water invasion layer of the shale gas reservoirs in different buried depths and at different fracture development conditions during hydraulic fracturing.

2.1. Experiment Samples

As shown in Figure 1, the two cylindrical core samples used in the water invasion simulation experiment were taken from Longmaxi Formation in Sichuan Basin. The specific parameters of the core samples are shown in Table 1.

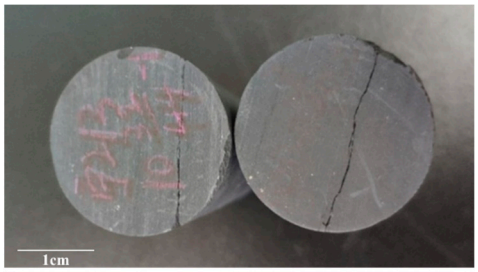

Figure 1. The two cylindrical core samples.

Table 1. Sample parameters.

Samples	Depth (m)	Porosity (%)	Diameter (cm)	Length (cm)	Dry Weight (g)	Density (kg/m^3)
N-1	3925	2.56	2.502	3.603	44.547	2.516
Z-1	3384	4.07	2.521	3.641	46.881	2.581

2.2. Experimental Equipment and Procedures

The experiment consists of two main stages: water invasion and CT scanning; the schematic diagrams of the water invasion experiment equipment and the CT scanning machine are shown in Figure 2. The liquid intermediate vessel is connected to the ISCO pump to provide the pressure, and the two core holders are connected in parallel to ensure that the same pressure is applied to the two core samples under the force of water during the water invasion. The patrol monitor apparatus is connected to the water invasion end of the core holder to monitor the pressure during the water invasion, and the hand piston pump is connected to the side end of the core holder to provide a stable confining pressure that is used to simulate the formation pressure in the shale gas reservoir. The experimental temperature was room temperature and the experimental pressure was 40 MPa.

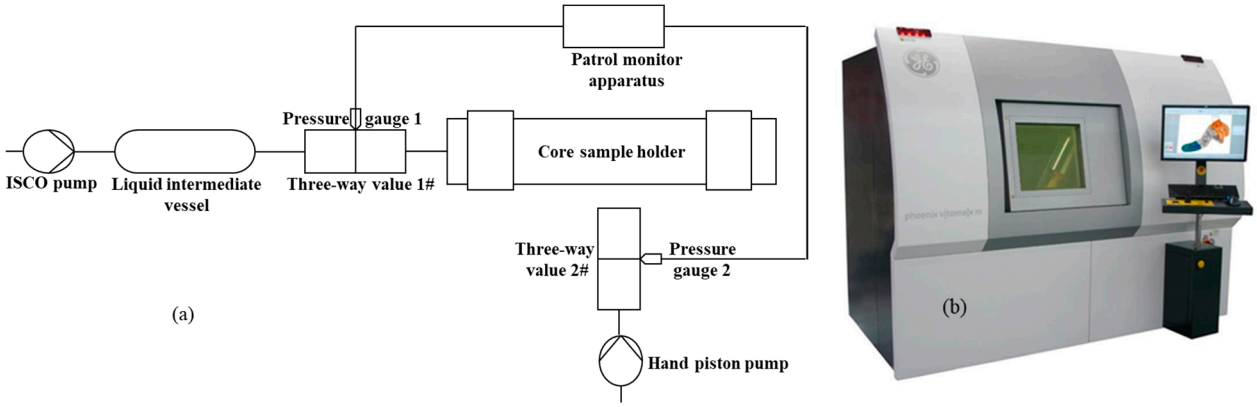

Figure 2. Flow diagram of water invasion experiment equipment (**a**) and CT scanning machine (**b**).

The experimental procedures were as follows:

1. CT scanning was performed on two dry core samples before the water invasion experiment.
2. The two core samples were placed respectively in the core holder, and the confining pressure was increased to 50 MPa by the hand piston pump and the water was increased to 40 MPa by the ISCO pump, and then water began to invade the two shale core samples.
3. After 24 h of water intrusion into the core samples, the ISCO pump pressure was removed first, and then the piston pump pressure was removed. The two core samples were taken out, and the surface moisture of the samples was wiped dry for the CT scan.
4. Steps (2) and (3) were repeated to obtain the CT scanning results of the shale core samples with a water intrusion time of 2 days, 4 days, and 6 days, respectively.
5. After CT scanning, the data were imported into Avizo software, and the core samples in different blocks and at different water invasion times were reconstructed in three dimensions, respectively, to obtain the scanning images of each section of the core sample to identify the pores and fractures.

2.3. Experimental Results and Discussion

The Avizo software, a professional graphic visual software, can be used to obtain the CT scanning results of the pore-fracture structure in different experimental stages to study the fracture propagation rule. Figures 3 and 4 show the two-dimensional section of different positions from the water intrusion end and the three-dimensional CT reconstruction and pore-fracture system before water invasion and after two, four, and six days of water invasion in the N-1 and Z-1 shale samples.

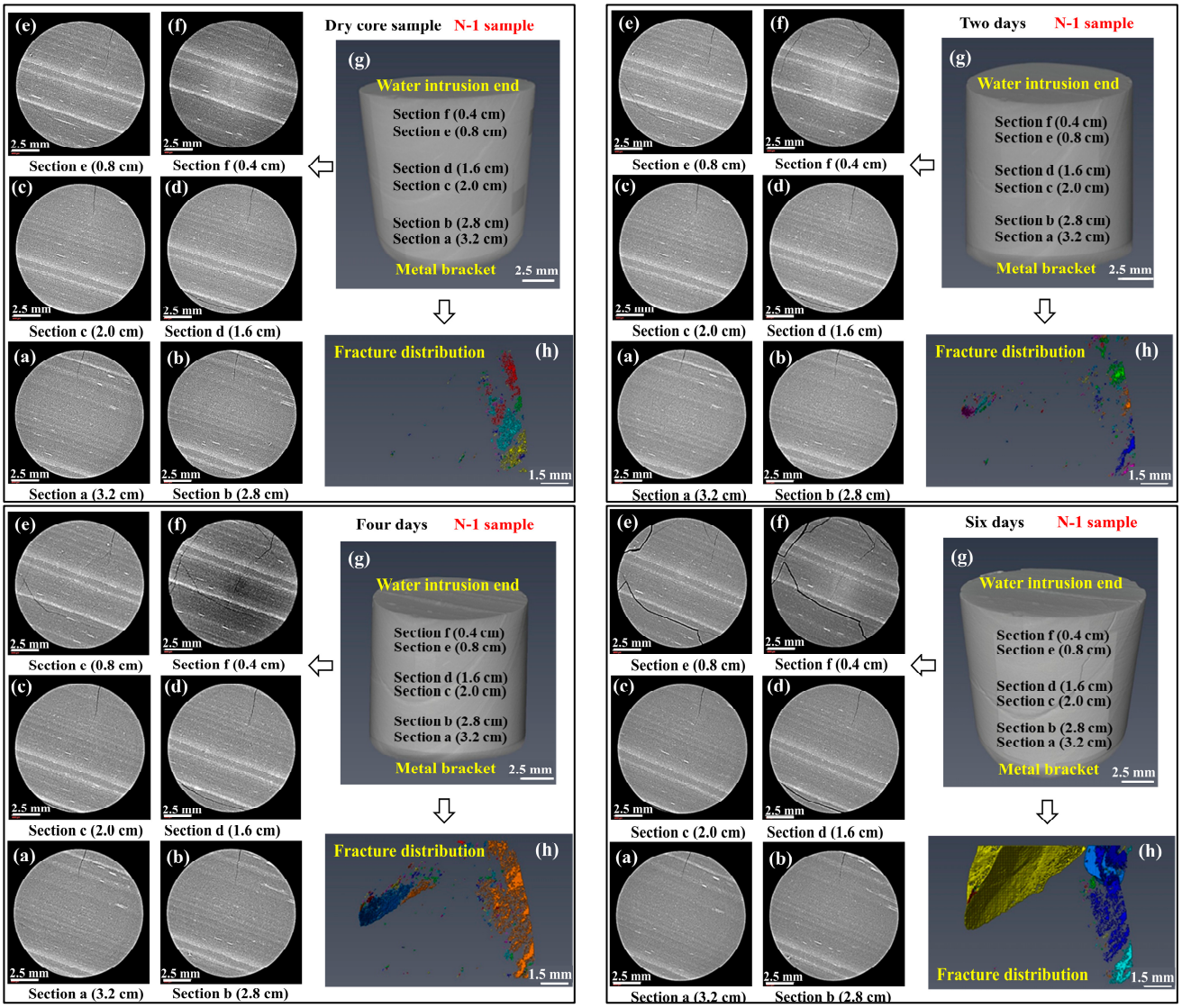

Figure 3. The CT images of the two-dimensional and three-dimensional pore-fracture systems in the N-1 sample before water invasion and after two, four, and six days of water invasion. (**a**–**f**) Two-dimensional section of different positions from the water intrusion end; (**g**) three-dimensional CT reconstruction of core sample; (**h**) three-dimensional pore-fracture system.

According to the CT scanning results of the samples before water invasion, it can be seen that the bedding of the N-1 sample is at an Angle of 45° with the Z-axis. There is a natural fracture parallel to the bedding plane at the water invasion end of the sample, and a microfracture running through the whole sample along the axial direction perpendicular to the bedding of the sample. The bedding of the Z-1 sample is parallel to the axial direction, and there are several natural fractures along the bedding direction. As can be seen from the CT scanning results of the samples after two days of water invasion, the width of the primary fracture at the water invasion end of the N-1 and Z-1 shale samples increased slightly, while some secondary fractures connected with them appeared, and the fractures far away from the water invasion end almost did not change. In addition, a small amount of rock fell off due to hydration at the edge of the water invasion end of the Z-1 sample. CT scanning results of the samples after four days of water invasion showed that the rock at the water invasion end of the N-1 sample began to fall off, and more rocks at the water invasion end of the Z-1 sample began to fall off. The fractures at the water invasion end of the N-1 and Z-1 samples were further developed, and the fracture width was further increased. A

large number of secondary fractures appeared and extended along the bedding direction. Microfractures developed far from the water invasion end, and the fracture width increased slightly. It was obvious that the fractures developed more than those from two days after the water invasion, as seen in the section image (d) at 1.6 cm away from the water invasion end. It can be seen from the CT scanning results of the samples after six days of water invasion that most rocks at the water invasion end of the N-1 and Z-1 shale samples were damaged, and a large number of edge rocks at the water invasion end of the samples began to fall off. The fractures at the water invasion end developed further, and a large number of secondary fractures were connected with each other, and the fracture width increased further. The microfractures developed further and the fracture width increased further, far from the water invasion end.

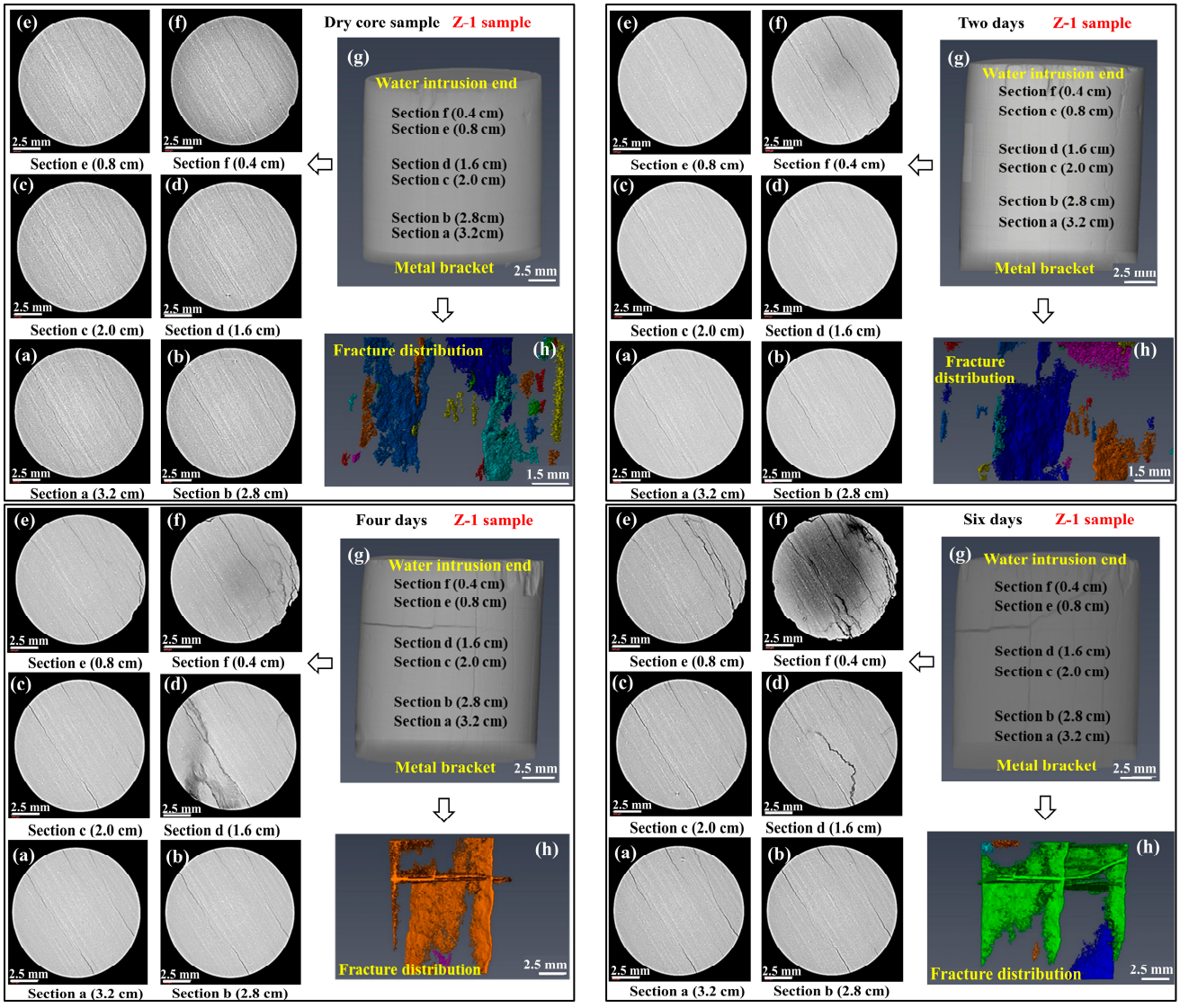

Figure 4. The CT images of the two-dimensional and three-dimensional pore-fractures system in the Z-1 sample before water invasion and after two, four, and six days of water invasion. (**a**–**f**) Two-dimensional section of different positions from the water intrusion end; (**g**) three-dimensional CT reconstruction of core sample; (**h**) three-dimensional pore-fracture system.

By analyzing the fracture morphology and matrix micro-damage in the two-dimensional section CT scanning images under different water invasion times, the water invasion frontier in the matrix and the thickness of the water invasion layer of the N-1 and Z-1 shale samples were determined, as shown in Figures 5 and 6. The ratio of thickness of the water

invasion layer to length of the core sample is defined as the dimensionless thickness of the water invasion layer. The thickness of the water invasion layer under different water invasion times is shown in Figure 7.

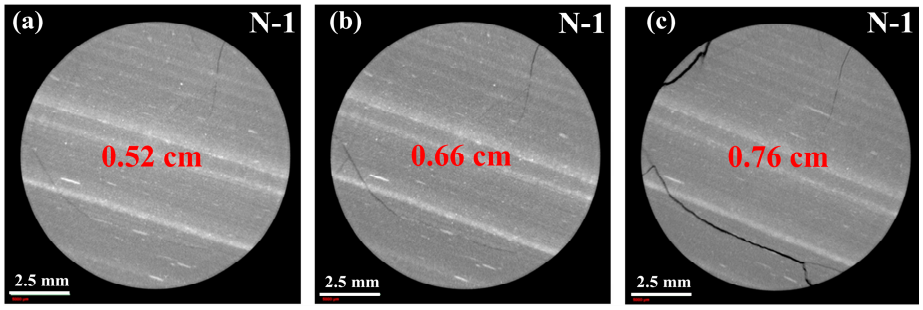

Figure 5. Schematic diagram of the water invasion frontier in the N-1 sample after various days of water invasion. (**a**) Two days after water invaded; (**b**) four days after water invaded; (**c**) six days after water invaded.

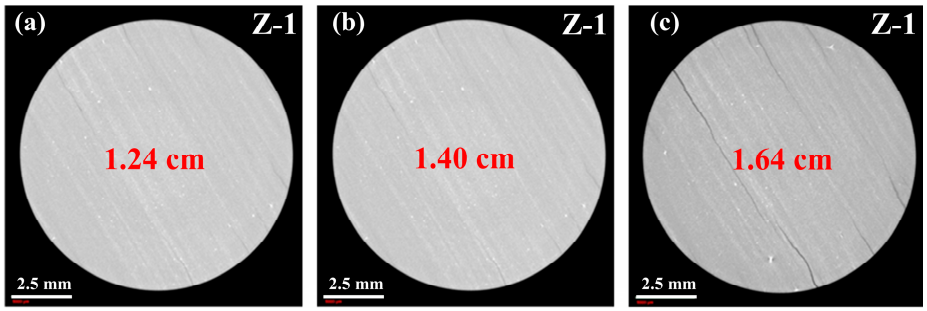

Figure 6. Schematic diagram of the water invasion frontier in the Z-1 sample after various days of water invasion. (**a**) Two days after water invaded; (**b**) four days after water invaded; (**c**) six days after water invaded.

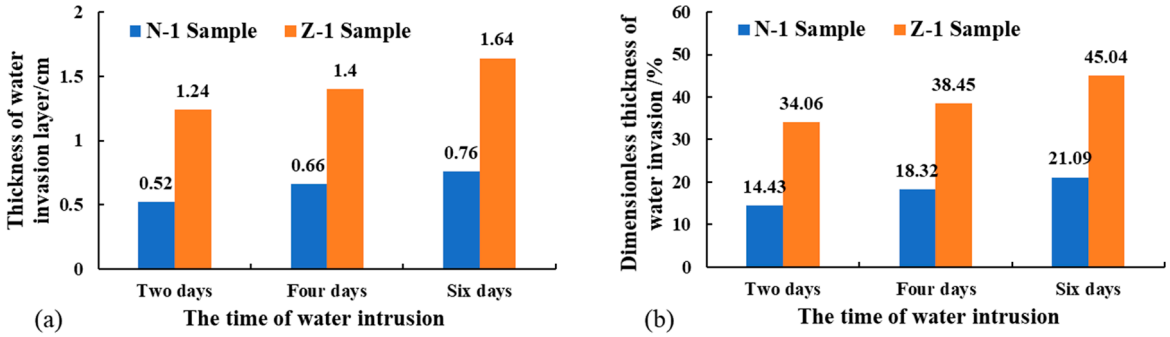

Figure 7. The thickness and dimensionless thickness of the water invasion layer of the N-1 and Z-1 shale samples. (**a**) Thickness of water invasion layer; (**b**) dimensionless thickness of water invasion layer.

Compared with the N-1 and Z-1 shale samples before and after water invasion in Figures 3 and 4, and the positions of the water invasion front in Figures 5 and 6, it can be seen that the primary fractures were more developed and the width of the fractures increased, and more secondary fractures were developed at the water invasion end of the core sample after water invasion. The thickness of the water invasion layer increases with the time of water intrusion. Although the thickness of the water invasion obtained by the experiment is only centimeter-level, it can be seen from the dimensionless thickness of the water invasion that 15–45% of the core sample is affected by water invasion in Figure 7.

Compared with the N-1 shale sample, the Z-1 shale sample is shallower in depth and has higher fracture development. After water invasion, the primary and secondary fractures are more developed, the rock damage at the water invasion end is more serious, and the water invasion layer is thicker. This is mainly due to the fact that deep shale has a tighter matrix and lower permeability, so the penetration depth of the fracturing fluid is smaller, the thickness of the water invasion layer is smaller, and the fracture propagation and microfracture generation are more difficult.

3. Numerical Simulations

3.1. Numerical Model

Laboratory experiments show that water invades shale samples from the end of water invasion, and the depth of water penetration varies with different shale samples and water invasion times. When multi-stage fractured horizontal wells are used to develop shale gas reservoirs, fracturing fluids first enter hydraulic fractures, then enter microfractures through hydraulic fractures and imbibition into the matrix. Therefore, the hydraulic fracture is equivalent to the water invasion end. Moreover, the depth of the fracturing fluid that intrudes into the matrix varies with different reservoirs and soaking times. It can be seen from the results of the water invasion experiment that the fracturing fluid can invade the matrix to a limited depth, and the fracturing fluid invasion will affect the properties of the shale samples, such as microfracture propagation to improve the porosity and permeability of shale samples near the water intrusion end. Therefore, in the numerical simulation model of a multi-stage fractured horizontal well for shale gas, a fracturing fluid invasion layer (FFIL) is added to the fracture surface to simulate the shale sample invaded by water near the water intrusion end in the water invasion experiment [38]. Furthermore, the permeability changes caused by microfracture propagation and formation damage were simulated by changing the FFIL permeability. The different penetration depths of the fracturing fluid into the matrix caused by different shale gas reservoirs and different soaking times were simulated by changing the FFIL thickness.

The commercial numerical simulation software tNavigator was used to establish the numerical simulation model, as shown in Figure 8. The shale gas reservoir is divided into the original reservoir volume and the stimulated reservoir volume, which is further divided into three areas: hydraulic fracture, FFIL, and matrix. The horizontal well is 1500 m long and fractured in 20 stages, and the total width of the model is 400 m. The horizontal well was first produced at a constant rate of 6×10^4 m^3/d, and then turned into constant pressure production when the pressure dropped to 5 MPa. The gas–water relative permeability curves in the hydraulic fracture and the FFIL, and the production curves, are shown in Figure 9. The values of the other parameters in the numerical simulation model are shown in Table 2.

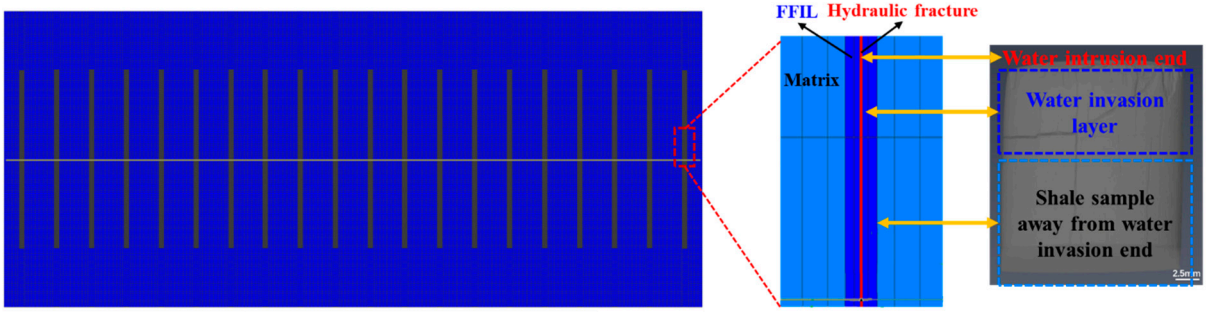

Figure 8. Schematic diagram of the numerical simulation model.

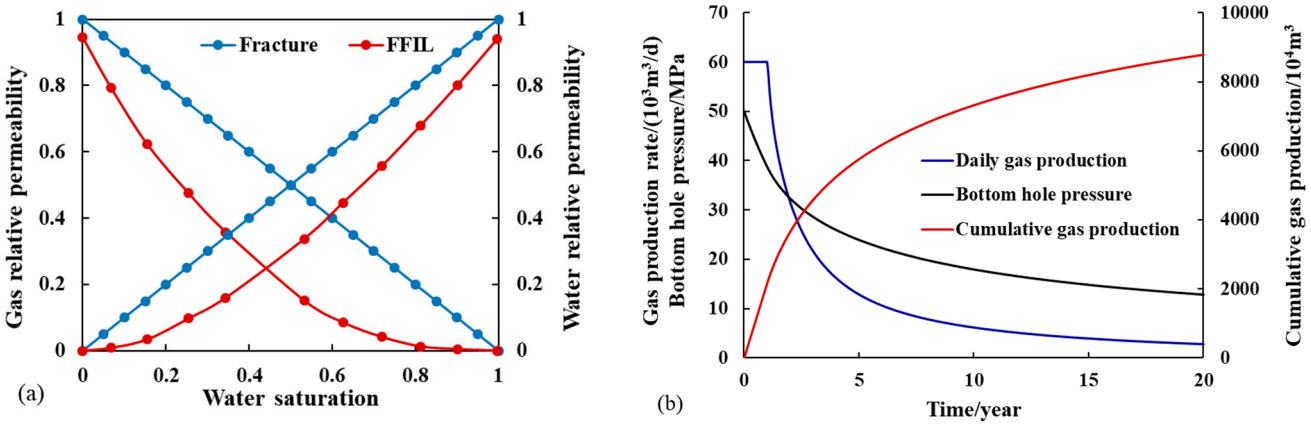

Figure 9. Gas–water relative permeability curves (**a**) and production curves (**b**).

Table 2. Model parameter values.

Parameters	Values	Parameters	Values
Initial formation pressure/MPa	50	Gas saturation/%	70
Initial formation temperature/K	373.15	Formation thickness/m	38
Permeability of matrix/10^{-3}μm^2	0.0005	Compression coefficient/MPa^{-1}	3×10^{-3}
Porosity/%	5	Shale density/(g/cm$^{3)}$	2.6
Half-length of fracture/m	120	Langmuir volume/(m^3/t)	3
Conductivity of fracture/(mD·m)	5	Langmuir pressure/MPa	6.5

3.2. Effect of Permeability of FFIL on Pressure and Gas Production

Both the negative effect of fracturing fluid retention on shale damage and the positive effect of microfracture formation and propagation exist in the flowback process of shale gas reservoirs after hydraulic fracturing. The positive effect of fracturing fluid retention is that the permeability increase of high-permeability samples is not significant, but it is more obvious for low permeability samples. If the negative effect of shale damage is offset, the permeability of a low-permeability shale sample is higher than its initial permeability, but the permeability of a high-permeability shale sample is still unable to recover completely.

The thickness of the FFIL is 20% of the thickness of the matrix block, and the permeability of the FFIL is 60%, 80%, 100%, 120%, and 140% of the matrix permeability, respectively. The ratio of FFIL permeability to matrix permeability is defined as the dimensionless FFIL permeability. When the dimensionless FFIL permeability is less than 1, it indicates that fracturing fluid retention has a more negative effect on shale damage. For example, the dimensionless FFIL permeability is 0.8, that is, the fracturing fluid intrusion causes 20% permeability damage to the reservoir; otherwise, it indicates that fracturing fluid retention has a greater positive effect on the reservoir. The influence of FFIL permeability on gas production and bottom-hole pressure of shale gas was studied through numerical simulation, and the results are shown in Figure 10.

As can be seen from Figure 10, the higher the dimensionless FFIL permeability, the longer the stable production period will be, and the greater the cumulative gas production during the stable production period will be. In the production decline stage, the larger the dimensionless FFIL permeability, the faster the gas production decline, the faster the pressure transfer, the faster the bottom-hole pressure drop, and the smaller the cumulative gas production will be in the decline stage. The gas production in the stable production period contributes more to the cumulative gas production. Under the same production time, the higher the dimensionless FFIL permeability, the smaller the increase in cumulative gas production will be. The permeability of the fracture has an obvious effect on the gas production rate at the initial period. With the increase in production time, reservoir pressure decreases and fracture permeability decreases, which makes less and less contribution to

gas production. Therefore, with the same dimensionless FFIL permeability, the production time increases and the cumulative gas production increases less and less.

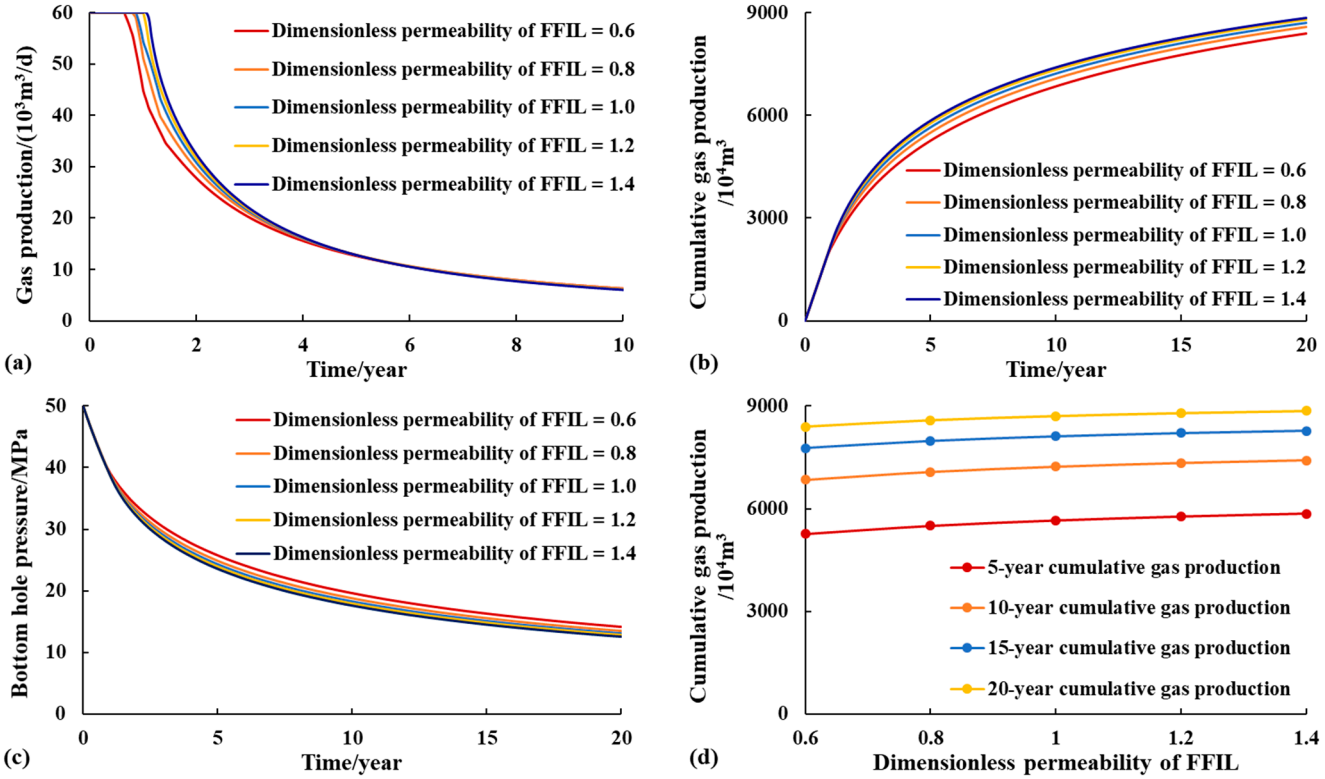

Figure 10. Effect of permeability of FFIL on gas production and pressure. (**a**) Effect of dimensionless permeability of FFIL on daily gas production; (**b**) effect of dimensionless permeability of FFIL on cumulative gas production; (**c**) effect of dimensionless permeability of FFIL on bottom-hole pressure; (**d**) cumulative gas production over 5, 10, 15, and 20 years at different permeabilities of FFIL.

In conclusion, the higher the dimensionless FFIL permeability, the more microfractures in the reservoir, the more complex the fracture network formed after hydraulic fracturing, the higher the cumulative gas production, and the better the development effect will be, which also explains the phenomenon of low flowback rate and high gas production after fracturing in some shale gas wells.

3.3. Effect of Thickness of FFIL on Pressure and Gas Production

During the hydraulic fracturing of shale gas wells, fracturing fluid can quickly enter the complex fracture network, and then slowly enter the shale matrix under the combined action of various mechanisms. The ratio of FFIL thickness to matrix block thickness is defined as the dimensionless FFIL thickness, and the relative depth of fracturing fluid intrusion into the matrix is characterized by the dimensionless FFIL thickness.

On the one hand, scholars have found that shale reservoirs with high clay content are easily damaged by the hydration and swelling of clay minerals [31,32], but on the other hand, Zhao et al. [39] found that clay minerals are also the main controlling factors of microfractures induced by shale hydration, and the increases in porosity and permeability are positively correlated with the clay content. The content of clay minerals in the S4 and S6 samples buried at 2400–2450 m is 52.2% and 35%, respectively. After imbibition at confining pressures of 12 MPa and 14 MPa for 5 days, the permeability increases 67.3 times and 17.6 times, and the porosity increases 1.63 times and 0.42 times, respectively.

In this paper, the depth of the N-1 sample is 3384 m, the pressure coefficient of the block is 1.1, the content of brittle minerals (quartz + feldspar + carbonate) is 66.3~88.1%, and the average content of clay minerals is 15.9%. The depth of the Z-1 sample is 3925 m, the

pressure coefficient of the block is 1.70–1.84, and the brittleness index is 48~62%, which is relatively high. The reservoir confining pressure has a prohibitive effect on shale imbibition, and the confining pressure in this experiment is 50 MPa. The N-1 and Z-1 shale samples had a large burial depth and were located in the lower Longmaxi Formation. Compared with the shallow shale samples, the clay mineral content is lower [40], and the fracture propagation is more difficult. In this paper, the increase in porosity after fracturing fluid invasion is too small to be ignored, and the change in permeability is mainly considered.

The N-1 and Z-1 samples have good fracability, which is conducive to the formation of complex fracture networks by hydraulic fracturing. It can also be seen from the water invasion experiment that abundant microfractures developed at the water invasion end after water invasion. Therefore, based on previous studies, it is considered that the positive effect on the fracturing fluid retention of the N-1 and Z-1 shale samples is greater, but the permeability increase times are much smaller than that of the shallow shale. The permeability of the FFIL is 120% of the matrix permeability, and the thickness of the FFIL is 10%, 20%, 30%, 40%, and 50% of the matrix block thickness, respectively. The influence of FFIL thickness on shale gas production and bottom-hole pressure is studied, and the results are shown in Figure 11.

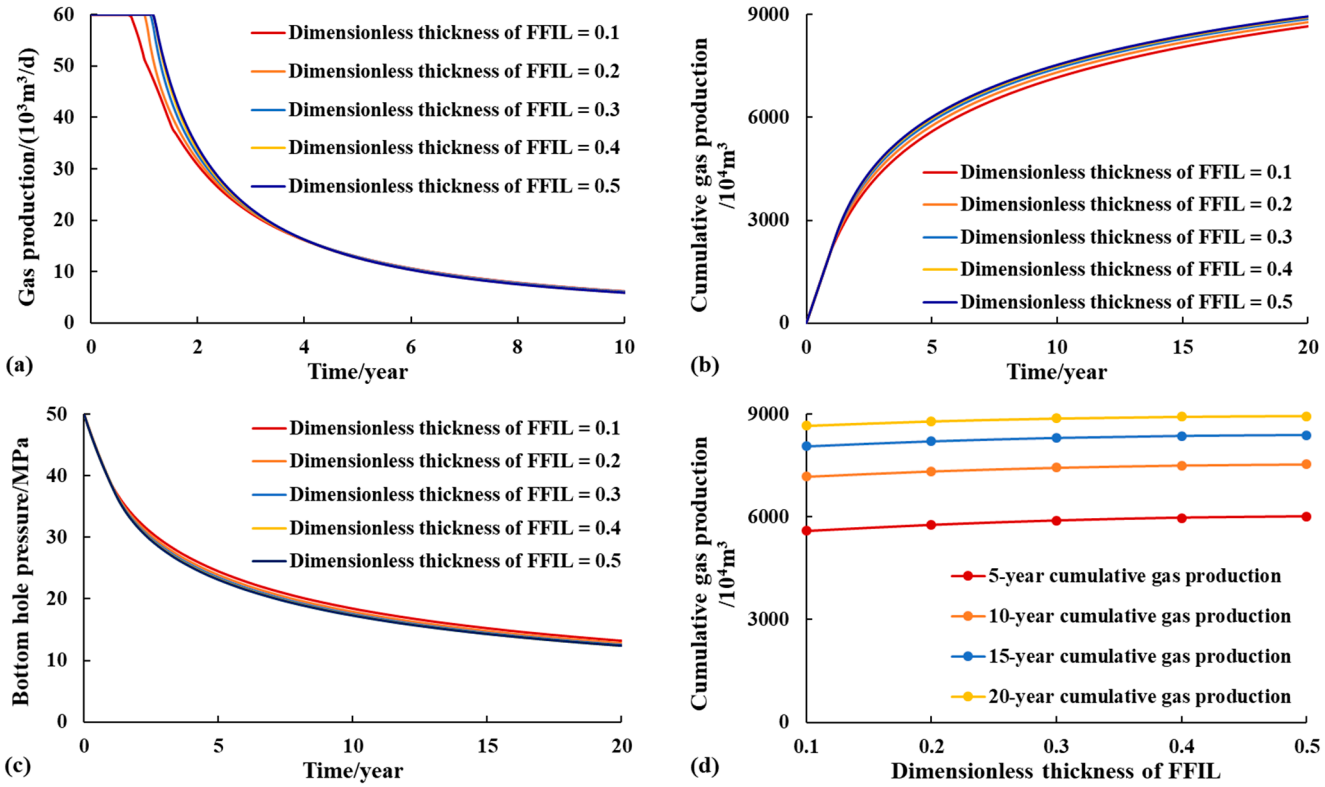

Figure 11. Effect of thickness of FFIL on gas production and pressure. (**a**) Effect of dimensionless thickness of FFIL on daily gas production; (**b**) effect of dimensionless thickness of FFIL on cumulative gas production; (**c**) effect of dimensionless thickness of FFIL on bottom-hole pressure; (**d**) cumulative gas production over 5, 10, 15, and 20 years at different thickness of FFIL.

As can be seen from Figure 11, the larger the dimensionless FFIL thickness, the more fracturing fluid retained in the reservoir is used to form microfractures, and the larger the expansion range of the microfractures, which is equivalent to the larger the dimensionless FFIL permeability, the longer the stable production period. The larger the dimensionless FFIL thickness, the longer the stable production period will be, and the larger the cumulative gas production will be during the stable production period; and the higher cumulative gas production, the better the development effect will be. Under the same production time, the greater the dimensionless FFIL thickness, the smaller the

increase in cumulative gas production. With the same dimensionless FFIL thickness, the cumulative gas production increases less and less as the production time increases.

On the basis of clarifying the impact of fracturing fluid retention on the reservoir, combined with the reservoir characteristics and fracture development, optimizing the soaking time and the speed of flowback of shale gas wells, in order to extend the stable production period, is the key to obtaining high productivity.

4. Discussion

In this study, the characteristics of the FFIL and its influence on productivity were studied by CT and numerical simulation experiments. The dimensionless thickness and permeability of the FFIL were used to characterize the different fracture propagation distance variations with different reservoirs and soaking times and the relative magnitude of the positive and negative effects of fracturing fluid retention on the shale gas reservoir. The influence of the complex mechanism behind fracturing fluid intrusion on seepage parameters was characterized by the dimensionless FFIL parameters. For example, the law of fracture propagation includes the orientation and distance of fracture propagation after fracturing fluid invasion, and the influence of fracturing fluid retention on the reservoir includes the hydration expansion of clay minerals and the permeability improvement caused by fracture propagation. On the one hand, the model does not need too many parameters to describe the complex mechanism, which is convenient for calculation and reliable conclusions. On the other hand, it is easier to perform sensitivity analysis and parameter optimization, which is convenient to optimize the flowback system.

However, if we want to describe more accurately the complex mechanism of fracturing fluid invasion, we need to further improve the experimental scheme and develop mathematical models to complement the shortcomings of commercial numerical simulation software. For example, this experimental instrument cannot quantitatively describe the fracture propagation process, so we can take a lesson from other research and take more factors into consideration, such as obtaining propagation length, opening width, and growing speed through high-speed imaging devices and image analysis software, and analyzing the influence of pore structure and natural fractures on fracture propagation [41,42], and the corresponding mathematical model needs to be established to describe and calculate it [43–45]. This would improve the quantitative analysis of the combined effects of fracturing fluid retention on fracture propagation and formation damage [46].

5. Conclusions

In this study, the fracturing fluid intrusion layer was introduced to study the influence of fracturing fluid retention on the reservoir through a CT scanning experiment and numerical simulation. Based on the results, the following conclusions were drawn:

1. The water invasion experiment confirmed that the retained fracturing fluid would induce microfracture propagation in the matrix, and the law and distance of fracture propagation were related to the original physical properties of the shale sample and the time of water invasion.
2. The shale samples used in the experiment are relatively dense with very low porosity and permeability, and the water intrusion thickness obtained at the core sample scale is only centimeter-level. However, it can be seen from the dimensionless water intrusion thickness that 15~45% of the core samples are affected by water intrusion.
3. Compared with a shallow shale reservoir, a deep shale reservoir has a denser matrix and lower permeability, so the penetration depth of fracturing fluid is smaller, the thickness of the fracturing fluid invasion layer is smaller, and fracture propagation is more difficult.
4. For shale gas wells, the positive and negative effects of fracturing fluid retention on the reservoir usually coexist, and dimensionless fracturing fluid invasion layer permeability was introduced to characterize the relative magnitude of the two effects. The higher the dimensionless fracturing fluid invasion layer permeability, the

more complex the fracture network formed after fracturing will be, resulting in a longer stable production period, a higher cumulative gas production, and a better development effect.

5. Dimensionless fracturing fluid invasion layer thickness was introduced to characterize the depth of fracturing fluid intrusion into the matrix. For low-permeability rock samples, the positive effect of fracturing fluid retention is greater, and the rock sample's permeability becomes higher than its initial permeability. In this case, the larger the dimensionless fracturing fluid invasion layer thickness, the more the fracturing fluid retained in the reservoir is used to form microfractures; and the larger the propagation range of the microfractures, the longer the stable production period, the greater the cumulative gas production, and the better the development effect will be.
6. The key to the efficient development of shale gas wells is to optimize the soaking time and flowback speed in combination with reservoir characteristics and fracture development, in order to maximize the positive effects and minimize the negative effects of fracturing fluid retention, and to extend the stable production period.

Author Contributions: Conceptualization, J.S. and S.H.; methodology, software and investigation, J.S. and J.Z.; writing—original draft preparation, J.S. and J.Z.; writing and editing, J.Z. and S.H.; supervision, F.Z. and X.D. All authors have read and agreed to the published version of the manuscript.

Funding: This study was funded by the National Natural Science Foundation of China (No. 51974328 and U19B6003-03-05).

Data Availability Statement: Not applicable.

Conflicts of Interest: The authors declare no conflict of interest.

References

1. Zou, C.; Zhao, Q.; Cong, L. Development progress, potential and prospect of shale gas in China. *Nat. Gas. Ind.* **2021**, *41*, 1–14.
2. Zhang, L.; He, X.; Li, X. Shale gas exploration and development in the Sichuan Basin: Progress, challenge and countermeasures. *Nat. Gas. Ind.* **2021**, *41*, 143–152. [CrossRef]
3. Warpinski, N.; Kramm, R.; Heinze, J. Comparison of single- and dual-array microseismic mapping techniques in the Barnett Shale. In Proceedings of the SPE Annual Technical Conference and Exhibition, Dallas, TX, USA, 9–12 October 2005. Available online: https://onepetro.org/SEGAM/proceedings/SEG05/All-SEG05/SEG-2005-1261/93122 (accessed on 6 April 2023).
4. Palisch, T.; Vincent, M.; Handren, P. Slickwater Fracturing: Food for Thought. *SPE Prod. Oper.* **2010**, *25*, 327–344. [CrossRef]
5. Javadpour, F.; Fisher, D.; Unsworth, M. Nanoscale Gas Flow in Shale Gas Sediments. *J. Can. Pet. Technol.* **2007**, *46*, 55–61. [CrossRef]
6. Wilson, A. Chemical Analysis of Flowback Water and Downhole Gas-Shale Samples. *J. Pet. Technol.* **2016**, *68*, 114–115. [CrossRef]
7. Ghanbari, E.; Abbasi, M.; Dehghanpour, H. Flowback volumetric and chemical analysis for evaluating load recovery and its impact on early-time production. In Proceedings of the SPE Unconventional Resources Conference Canada, Calgary, AL, Canada, 5–7 November 2013. [CrossRef]
8. Clarkson, C.; Williams-Kovacs, J. Modeling Two-Phase Flowback of Multifractur ed Horizontal Wells Completed in Shale. *SPE J.* **2013**, *18*, 795–812. [CrossRef]
9. Shaoul, J.; Van Zelm, L.; De Pater, C. Damage Mechanisms in Unconventional-Gas-Well Stimulation—A New Look at an Old Problem. *SPE Prod. Oper.* **2011**, *26*, 388–400.
10. Huang, Z. Research on Mechanisms of Retention and Flowback of Fracturing Fluids in Artificial Fracture Network. Master's Thesis, China University of Petroleum, Beijing, China, 2019.
11. Song, B. Model for Fracturing Fluid Flowback and Characterization of Flowback Mechanisms. Ph.D. Thesis, Texas A & M University, College Station, TX, USA, 2014. Available online: https://oaktrust.library.tamu.edu/bitstream/handle/1969.1/153854/SONG-DISSERTATION-2014.pdf (accessed on 6 April 2023).
12. McClure, M. The potential effect of network complexity on recovery of injected fluid following hydraulic fracturing. In Proceedings of the SPE Unconventional Resources Conference, The Woodlands, TX, USA, 1–3 April 2014. [CrossRef]
13. Agrawal, S.; Sharma, M. Liquid loading within hydraulic fractures and its impact on unconventional reservoir productivity. In Proceedings of the Unconventional Resources Technology Conference, Denver, CO, USA, 12–14 August 2013. [CrossRef]
14. Parmar, J.; Dehghanpour, H.; Kuru, E. Displacement of water by gas in propped fractures: Combined effects of gravity, surface tension, and wettability. *J. Unconv. Oil Gas Resour* **2014**, *5*, 10–21. [CrossRef]
15. Liu, Y. Modeling of Recovery and In-situ Distribution of Fracturing Fluid in Shale Gas Reservoirs Due to Fracture Closure, Proppant Distribution and Gravity Segregation. Master's Thesis, University of Alberta, Edmonton, AL, Canada, 2017. [CrossRef]

16. Parmar, J.; Dehghanpour, H.; Kuru, E. Drainage Against Gravity: Factors Impacting the Load Recovery in Fractures. In Proceedings of the SPE Unconventional Resources Conference-USA, The Woodlands, TX, USA, 10–12 April 2013. [CrossRef]
17. Cheng, Y. Impact of Water Dynamics in Fractures on the Performance of Hydraulically Fractured Wells in Gas-Shale Reservoirs. *J. Can. Pet. Technol.* **2012**, *51*, 143–151. [CrossRef]
18. Penny, G.; Pursley, J.; Clawson, T. Field Study of Completion Fluids to Enhance Gas Production in the Barnett Shale. In Proceedings of the SPE Gas Technology Symposium, Calgary, AL, Canada, 15–17 May 2006. [CrossRef]
19. King, G. Thirty years of gas shale fracturing: What have we learned? In Proceedings of the SPE Annual Technical Conference and Exhibition, Florence, Italy, 19–22 September 2010. [CrossRef]
20. Warpinski, N.; Mayerhofer, M.; Vincent, M. Stimulating Unconventional Reservoirs: Maximizing Network Growth While Optimizing Fracture Conductivity. *J. Can. Pet. Technol.* **2009**, *48*, 39–51. [CrossRef]
21. McClure, M.; Horne, R. Correlations between formation properties and induced seismicity during high pressure injection into granitic rock. *Eng. Geol.* **2014**, *175*, 74–80. [CrossRef]
22. Modeland, N.; Buller, D.; Chong, K. Statistical analysis of the effect of completion methodology on production in the Haynesville Shale. In Proceedings of the North American Unconventional Gas Conference and Exhibition, The Woodlands, TX, USA, 14–16 June 2011. [CrossRef]
23. Chang, L. Study on Interaction Mechanism between Unsaturated Shale with Fractures and Fluid. Ph.D. Thesis, China University of Petroleum, Beijing, China, 2019. [CrossRef]
24. Dehghanpour, H.; Lan, Q.; Saeed, Y. Spontaneous Imbibition of Brine and Oil in Gas Shales: Effect of Water Adsorption and Resulting Microfractures. *Eng. Fuels* **2013**, *27*, 3039–3049. [CrossRef]
25. Roshan, H.; Ehsani, S.; Marjo, C. Mechanisms of water adsorption into partially saturated fractured shales: An experimental study. *Fuel* **2015**, *159*, 628–637. [CrossRef]
26. Meng, M.; Ge, H.; Ji, W. Investigation on the variation of shale permeability with spontaneous imbibition time: Sandstones and volcanic rocks as comparative study. *J. Nat. Gas Sci. Eng.* **2015**, *27*, 1546–1554. [CrossRef]
27. Meng, M.; Ge, H.; Ji, W. Research on the auto-removal mechanism of shale aqueous phase trapping using low field nuclear magnetic resonance technique. *J. Petrol. Sci. Eng.* **2016**, *137*, 63–73. [CrossRef]
28. Lv, F. Interacions between shale reservoir and fracturing fluid in Southern Sichuan. Master's Thesis, China University of Petroleum (East China), Qingdao, China, 2019. [CrossRef]
29. Liu, Y.; Leung, J.; Chalaturnyk, R. New Insights on Mechanisms Controlling Fracturing-Fluid Distribution and Their Effects on Well Performance in Shale-Gas Reservoirs. *SPE Prod. Oper.* **2019**, *34*, 564–585. [CrossRef]
30. Kang, Y.; Zhang, X.; You, L. The experimental research on spontaneous flowbackrelieving aqueous phase trapping damage in shale gas reservoirs. *Nat. Gas. Geosci.* **2017**, *28*, 819–827.
31. Zhou, T.; Zhang, S.; Yang, L. Experimental investigation on fracture surface strength softening induced by fracturing fluid imbibition and its impacts on flow conductivity in shale reservoirs. *J. Nat. Gas Sci. Eng.* **2016**, *36*, 893–905. [CrossRef]
32. Zhou, Z.; Teklu, T.; Li, X. Experimental study of the osmotic effect on shale matrix imbibition process in gas reservoirs. *J. Nat. Gas Sci. Eng.* **2018**, *49*, 1–7. [CrossRef]
33. Liu, X.; Xiong, J.; Liang, L. Hydration Experiment of Hard Brittle Shale of the Longmaxi Formation. *J. Southwest Petrol. Univ. Nat. Sci. Ed.* **2016**, *38*, 178–186.
34. Zhang, J.; Zhu, D.; Hill, A. Water-induced fracture conductivity damage in shale formations. In Proceedings of the SPE Hydraulic Fracturing Technology Conference, The Woodlands, TX, USA, 3–5 February 2015. [CrossRef]
35. Rouchaudhuri, B.; Tsotsis, T.; Jessen, K. Shale-fluid interactions during forced lmbibition and flow-back. *J. Petrol. Sci. Eng.* **2019**, *172*, 443–453. [CrossRef]
36. Singh, H. A critical review of water uptake by shales. *J. Nat. Gas. Sci. Eng.* **2016**, *34*, 751–766. [CrossRef]
37. You, L.; Cheng, Q.; Kang, Y. Experimental study on spontaneous water imbibition in fracture networks of shale rocks. *J. China Univ. Pet. Nat. Sci. Ed.* **2016**, *38*, 178–186.
38. Wu, Y.; Cheng, L.; Ma, L. A transient two-phase flow model for production prediction of tight gas wells with fracturing fluid-induced formation damage. *J. Petrol. Sci. Eng.* **2021**, *199*, 108351. [CrossRef]
39. Zhao, Z.; He, Y.; Guo, J.; Zheng, X.; Tao, L.; Deng, X. Experimental Study on the Forcible Imbibition Law of Water in Shale Gas Reservoirs. *Processes* **2023**, *11*, 1057. [CrossRef]
40. Xu, L.; Huang, S.; Sun, M.; Wen, Y.; Chen, W.; Zhang, Y.; Luo, F.; Zhang, H. Palaeoenvironmental Evolution Based on Elemental Geochemistry of the Wufeng-Longmaxi Shales in Western Hubei, Middle Yangtze, China. *Minerals* **2023**, *13*, 502. [CrossRef]
41. Jin, Z.; Johnson, S.E.; Fan, Z.Q. Subcritical propagation and coalescence of oil-filled cracks: Getting the oil out of lowpermeability source rocks. *Geophys. Res. Lett.* **2010**, *37*, L01305. [CrossRef]
42. Fan, Z.; Jin, Z.; Johnson, S. Modelling petroleum migration through microcrack propagation in transversely isotropic source rocks. *Geophys. J. Int.* **2012**, *190*, 179–187. [CrossRef]
43. Makarova, A.; Kaliberda, I.; Kovalev, D. Modeling a production well flow control system using the example of the Verkhneberezovskaya Area. In Proceedings of the 2022 Conference of Russian Young Researchers in Electrical and Electronic Engineering (ElConRus), Saint Petersburg, Russia, 25–28 January 2022. [CrossRef]

44. Makarova, A.; Mantorova, I.; Kovalev, D. The modeling of mineral water fields data structure. In Proceedings of the 2021 IEEE Conference of Russian Young Researchers in Electrical and Electronic Engineering (ElConRus), Saint Petersburg/Moscow, Russia, 26–29 January 2021. [CrossRef]
45. Martirosyan, A.; Ilyushin, Y. Modeling of the Natural Objects' Temperature Field Distribution Using a Supercomputer. *Informatics* **2022**, *9*, 62. [CrossRef]
46. Lyons Cerón, A.; Konist, A. Co-Pyrolysis of Woody Biomass and Oil Shale in a Batch Reactor in CO_2, CO_2-H_2O, and Ar Atmospheres. *Energies* **2023**, *16*, 3145. [CrossRef]

Disclaimer/Publisher's Note: The statements, opinions and data contained in all publications are solely those of the individual author(s) and contributor(s) and not of MDPI and/or the editor(s). MDPI and/or the editor(s) disclaim responsibility for any injury to people or property resulting from any ideas, methods, instructions or products referred to in the content.